A study of metal-MoS2 contacts by using an in-house developed ab-initio transport simulator

Daniel Lizzit, Pedram Khakbaz, Francesco Driussi, Marco G. Pala, David Esseni

A study of metal-MoS_2 contacts by using an in-house developed *ab-initio* transport simulator

Daniel Lizzit[a,*], Pedram Khakbaz[a], Francesco Driussi[a], Marco Pala[b], David Esseni[a]

[a] *DPIA, University of Udine, Via delle Scienze 206, 33100 Udine, Italy*
[b] *Université Paris-Saclay, CNRS, C2N, F-91120 Palaiseau, France*

Abstract

By combining DFT calculations and an in-house developed, *ab-initio* transport simulator, we investigate the transport properties of n-type contacts between 3D metallic conductors and monolayer MoS_2. Moreover, the impact of buffer layers between the metal and the MoS_2 is also analyzed in order to reduce the Schottky barrier and approach the Ohmic behavior of contacts.

Keywords: MoS_2, DFT, NEGF, buffer layers, Schottky barrier, Tunneling barrier.

1. Introduction

Two dimensional (2D) semiconductors (SC) are actively investigated for applications in many fields spreading from tactile sensing in soft robotics [1, 2, 3], fast thermal sensors [4], and beyond silicon CMOS circuits [5].

However, many prospective applications are presently hindered by the lack of low resistance Ohmic contacts. One major difficulty stems from a persistent Fermi level pinning (FLP), that leads to a weak modulation of the experimentally observed Schottky barrier height (SBH) with the metal work function (WF) [6, 7]. Although defective metal-SC interfaces are in part responsible for

*Corresponding author
Email addresses: daniel.lizzit@uniud.it (Daniel Lizzit), khakbaz.pedram@spes.uniud.it (Pedram Khakbaz), francesco.driussi@uniud.it (Francesco Driussi), marco.pala@c2n.upsaclay.fr (Marco Pala), david.esseni@uniud.it (David Esseni)

the FLP observed in experiments, even atomically perfect interfaces show a significant SBH due to metal-induced-gap-states (MIGS) [8, 9], which degrade the contact resistance and the current drivability.

A possible means to alleviate the FLP is to reduce the MIGS by increasing the metal-SC distance with the insertion of buffer layers [10, 11, 12], even though the effectiveness of this approach strongly depends on the metal-buffer layer atomic species [13]. Nevertheless, the reduction of FLP comes at the cost of a larger tunnelling barrier (TB) in the van der Waals gap, so that the state-of-the-art resistance for metal-TMD contacts has been close to 1 k$\Omega\cdot\mu$m in recent years, namely much larger than in metal-Si contacts. Only very recent experimental results by using the semi-metal Bismuth to contact MoS_2 have reported a smaller value of about 123 $\Omega\cdot\mu$m [14].

In this work we consider monolayer MoS_2 in contact with a CMOS compatible, low work function metal (Aluminum) to obtain an n-type Ohmic contact, whereby the transport properties were investigated by using the *ab-initio* Non-Equilibrium Green's Function (NEGF) formalism presented in [15], in the ballistic regime. Our simulation approach allowed us to examine the behavior of metal-MoS_2 vertical contacts long tens on nanometers, still retaining the rigor of *ab-initio* calculations.

2. Simulation methodology

Al-MoS_2 vertical heterojunctions (VHJ) (including also buffer layers such as graphene (Gr) or hBN) were investigated with the Density Functional Theory (DFT) by using the Quantum ESPRESSO (QE) suite [16].

Figure 1 shows the super-cell and the atomic arrangement of an Al-MoS_2 VHJ with a Gr buffer layer. QE simulations were used to perform a complete geometry optimization making the metal and Gr layers commensurate to the MoS_2 as it is better explained in[17].

Ab-initio transport calculations are performed for a heterogeneous system consisting of an Al region, the VHJ and an MoS_2 region, arranged in the overall

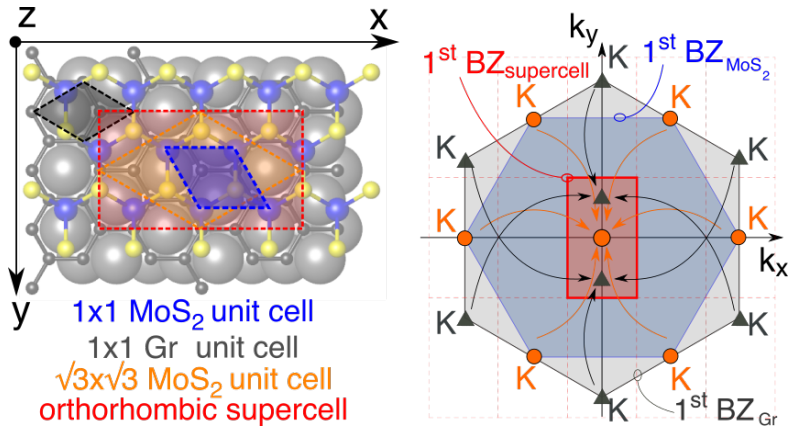

Figure 1: *left)* Orthorhombic supercell used for the transport simulation of the Al-Gr-MoS_2 VHJ where a six-layer Al crystal is matched to a $\sqrt{3}\times\sqrt{3}$ MoS_2 supercell. *right)* First Brillouin zones (1^{st}BZ) for the primitive MoS_2 unit cell (blue hexagon) and Gr unit cell (black hexagon), and 1^{st}BZ for the orthorhombic supercell (red rectangle). Arrows show the backfolding of MoS_2 and Gr K-points in the 1^{st}BZ of the supercell.

structure shown in Fig. 2. Each of these regions include several orthorhombic unit cells resulting in a simulated structure with thousands of atoms. To overcome the problem of very computationally demanding *ab-initio* transport calculations, we first reduced the size of the plane-wave DFT Hamiltonians thanks to a transformation to the hybrid basis $x\mathbf{K}_{yz}$ space (consisting of real-space along the transport direction x and plane waves in the (y,z) directions), and then to a basis set consisting of unit-cell restricted Bloch functions, as it was described for homogenous systems in [15]. The connection between the different materials is obtained by using Hamiltonian blocks describing the coupling between the two adjacent systems. Finally, the electronic transmission and the current through the VHJ are calculated by using the NEGF formalism [15].

3. Band structure and SBH

At the minimum energy distance (MED), the electronic structure of the Al-MoS_2 VHJ supercell projected on MoS_2 is shown in Fig. 3a, and it looks strongly perturbed by the Al to MoS_2 interaction, compared with the electronic

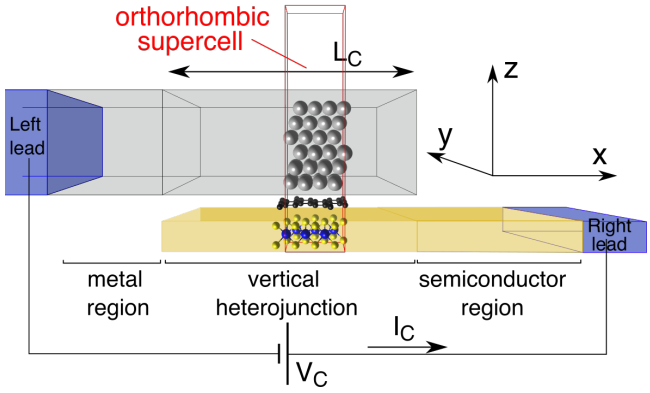

Figure 2: Sketch of the simulated structure with metal, VHJ (with Gr buffer layer) and semiconductor regions and consisting of several replicas of the super cells along x.

structure of free-standing MoS_2 (Fig. 3b). The presence of MIGS states due to the Al to MoS_2 interaction results in FLP and in a SBH of ∼0.25 eV, that is consistent with [17].

The introduction of a Gr buffer layer (Fig. 4a) leads to an increase of the SBH to ∼500 meV. Unlike the Al-MoS_2 VHJ, this is not related to the presence of MIGS, as it can be seen from the absence of MoS_2-related states in the SC band gap, but it stems instead from the charge transfer between Al and Gr. Indeed, the Gr Dirac cone (Fig. 4a, black circles) that is located along the Y-Γ high symmetry points of the orthorhombic supercell BZ (consistently with the bands projection shown in Figs. 1-*right* and 3b), is shifted by ∼500meV below the FL indicating that Gr is charged with electrons. This value is very close to the 0.57 eV calculated for the graphene/Al(111) stack alone [18], and similar to the experimental findings for the graphene/Al/Ni(111) system [19]. The Gr buffer layer shields the charge transfer from Al to MoS_2 leaving the MoS_2 almost uncharged, as demonstrated by the FL located well inside the MoS_2 band gap. An estimate of the Al to Gr charge transfer can be obtained from the energy dispersion relation of Fig. 4a, that allows us to derive a Fermi velocity v_F∼8×10^7 cm/s. Then, considering the Gr degeneracy of about δ∼500 meV, we can infer a Gr electron charging of N_{Gr}∼4×10^{13} cm^{-2} according to

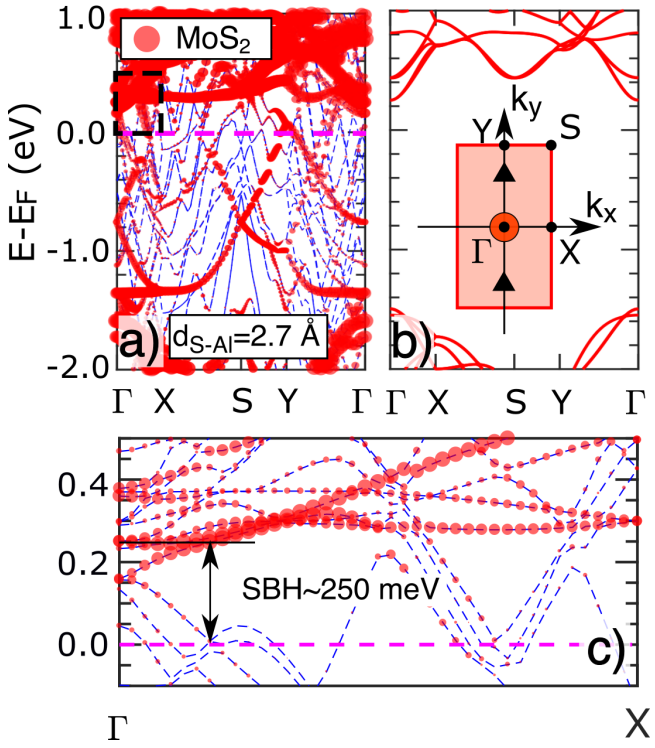

Figure 3: a) Electronic structure for the Al-MoS_2 orthorhombic VHJ. The size of circles is proportional to the weight of the bands projection onto MoS_2 orbitals. Dashed lines are non-orbital-projected bands. The Sulfur-Al distance is reported. Horizontal dashed line is the Fermi energy. b) Free standing MoS_2 band structure; bands are aligned such to obtain the same SBH as in a). The inset shows high symmetry points for the orthorombic supercell shown in Fig. 1, where the circle at the Γ-point denotes the MoS_2 conduction band minima and triangles denote the position of the Gr Dirac point when a Gr buffer layer is used. c) Zoom of the electronic structure corresponding to the dashed square in a) with an estimate of the SBH.

the simplified 0 K expression for the Gr charge density [20]:

$$N_{Gr} = \frac{\delta^2}{\pi \hbar^2 v_F^2} \tag{1}$$

where $\hbar$ is the reduced Planck's constant. These results suggest that a Gr buffer layer can effectively weaken the metal-SC interaction and prevent the formation of MIGS, but its electrostatic shielding effect tends to increase the Al-MoS_2 SBH. However, it has to be noticed that the Gr insertion does not

always increase the SBH, in fact the metal-to-Gr charge transfer depends on the metal atomic species [13].

We therefore investigated the impact of another atomically thin buffer layer, namely the monolayer hexagonal boron-nitride (hBN) having insulating properties. The hBN buffer layer can effectively suppress the MIGS (Fig. 4b) and the FLP, thus reducing the SBH down to 9 meV, but at the cost of a thicker TB (d=7.1 $\AA$) with respect to the MED case.

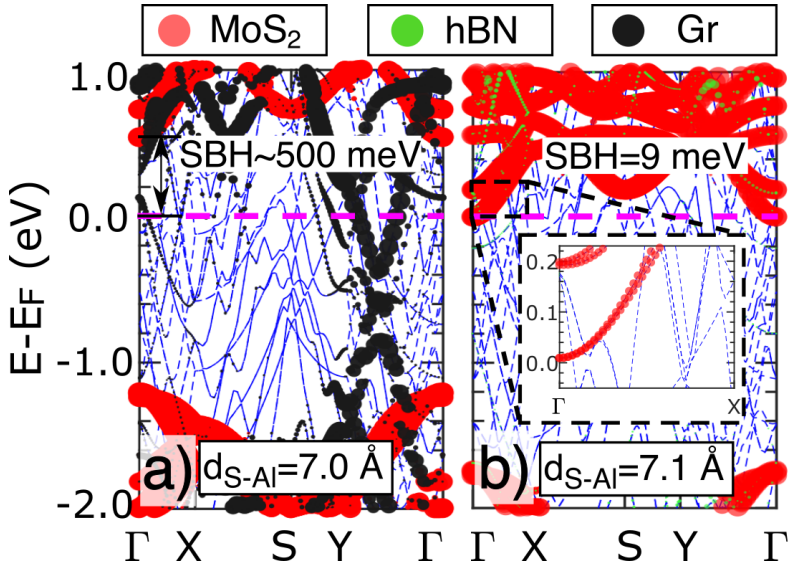

Figure 4: Electronic structure for a) Al-Gr-MoS_2 and b) Al-hBN-MoS_2. Inset: zoom-in near the minimum of the MoS_2 conduction band.

4. Transport simulations

Transport simulations in this work require to set the alignment between the conduction band minimum of the free standing MoS_2 (rightmost region in Fig. 2) and the MoS_2 projected bands in the VHJ (see Figs. 3 and 5). Such an alignment of the energy levels is sound and viable as long as the MoS_2 projected bands in the VHJ can be unambiguously identified, which in turn requires a weak metal-SC orbital hybridization. For this reason, we skipped transport

simulations for the Al-MoS_2 VHJ shown in Fig. 3a, given the strong MoS_2 orbital hybridization. The influence on the results of such a band alignment is emphasized by the fact that, at present stage, our simulations do not include a self-consistent solution of the transport and Poisson equations. Figure 5 shows the current I_C through contact versus the voltage V_C across the Al-hBN-MoS_2 stack obtained from NEGF simulations. The small V_C range splits the Fermi energies of the left and right leads (see Fig. 2) into $\pm qV_C/2$. As it can be seen, the contact is practically Ohmic at 300 K, whereas at 15 K a rectifying behavior is observed due to the 9 meV SBH. These results are consistent with experiments reported for MOSFET-like devices featuring the same contact stack and in the same temperature range [12]. The extracted contact resistance at 300 K is R_C=1.5 k$\Omega\cdot\mu$m, namely still about 10 times larger than in high quality Si-metal contacts.

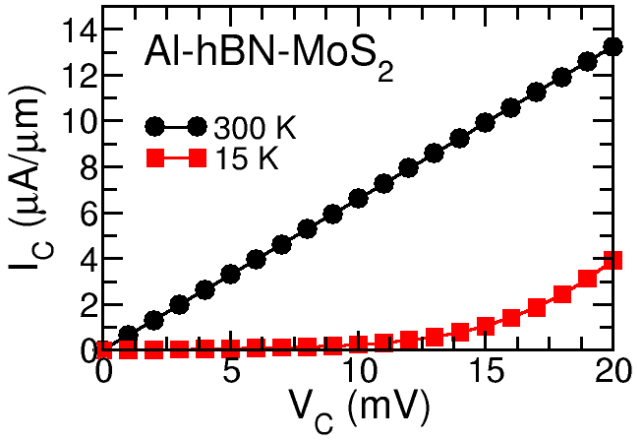

Figure 5: Simulated I_C versus V_C for the Al-hBN-MoS_2 VHJ with L_C=28.5 nm (30 orthorhombic super cells, see Fig. 2).

5. Conclusions

We have used an in house developed, ab initio transport methodology to investigate Al-MoS_2 contacts. We obtained a fairly Ohmic behavior at room temperature by using an hBN buffer layer, but the contact resistance is still

high compared to state of the art metal-Si contacts. This methodology can be naturally extended to other (semi)metal-TMD systems. Moreover, the simulation methodology can be improved by introducing a self-consistent calculation of a potential drop along the transport direction and by introducing dissipative transport effects according to the NEGF formalism.

6. Acknowledgements

This work was supported by the Italian MIUR through the PRIN Project 2017SRYEJH and the French ANR through the project "2D-on-Demand" (n. ANR-20-CE09-0026).

References

[1] A. Chortos, J. Liu, Z. Bao, Pursuing prosthetic electronic skin, Nature Materials 15 (2016) 937—-950. doi:10.1038/nmat4671.

[2] M. Hosseini, M. Elahi, M. Pourfath, D. Esseni, Strain-Induced Modulation of Electron Mobility in Single-Layer Transition Metal Dichalcogenides MX_2 (M=Mo, W; X = S,Se), IEEE Transactions on Electron Devices 62 (10) (2015) 3192–3198. doi:10.1109/TED.2015.2461617.

[3] Y. J. Park, B. K. Sharma, S. M. Shinde, M.-S. Kim, B. Jang, J.-H. e. a. Kim, All MoS_2-Based Large Area, Skin-Attachable Active-Matrix Tactile Sensor, ACS Nano 13 (3) (2019) 3023–3030. doi:10.1021/acsnano.8b07995.

[4] A. I. Khan, P. Khakbaz, K. A. Brenner, K. K. Smithe, M. J. Mleczko, D. e. a. Esseni, Large temperature coefficient of resistance in atomically thin two-dimensional semiconductors, Applied Physics Letters 116 (20) (2020) 203105. doi:10.1063/5.0003312.

[5] G. Iannaccone, F. Bonaccorso, L. Colombo, G. Fiori, Quantum engineering of transistors based on 2D materials heterostructures, Nature Nanotechnology 13 (3) (2018) 183–191. doi:10.1038/s41565-018-0082-6.

[6] A. Allain, J. Kang, K. Banerjee, A. Kis, Electrical contacts to two-dimensional semiconductors, Nature Materials 14 (12) (2015) 1195–1205. doi:10.1038/nmat4452.

[7] C. Kim, I. Moon, D. Lee, M. S. Choi, F. Ahmed, S. e. a. Nam, Fermi Level Pinning at Electrical Metal Contacts of Monolayer Molybdenum Dichalcogenides, ACS Nano 11 (2) (2017) 1588–1596. doi:10.1021/acsnano.6b07159.

[8] J. Kang, W. Liu, D. Sarkar, D. Jena, K. Banerjee, Computational Study of Metal Contacts to Monolayer Transition-Metal Dichalcogenide Semiconductors, Phys. Rev. X 4 (2014) 031005. doi:10.1103/PhysRevX.4.031005.

[9] M. Farmanbar, G. Brocks, First-principles study of van der Waals interactions and lattice mismatch at MoS_2/metal interfaces, Phys. Rev. B 93 (2016) 085304. doi:10.1103/PhysRevB.93.085304.

[10] M. Farmanbar, B. Geert, Ohmic Contacts to 2D Semiconductors through van der Waals Bonding, Advanced electronic materials 2 (4) (2016) 1500405. doi:10.1002/aelm.201500405.

[11] Y. Du, L. Yang, J. Zhang, H. Liu, K. Majumdar, P. D. e. a. Kirsch, MoS_2 Field-Effect Transistors With Graphene/Metal Heterocontacts, IEEE Electron Device Letters 35 (5) (2014) 599–601. doi:10.1109/LED.2014.2313340.

[12] X. Cui, E.-M. Shih, L. A. Jauregui, S. H. Chae, Y. D. Kim, B. e. a. Li, Low-Temperature Ohmic Contact to Monolayer MoS_2 by van der Waals Bonded Co/h-BN Electrodes, Nano Letters 17 (8) (2017) 4781–4786. doi:10.1021/acs.nanolett.7b01536.

[13] A. Chanana, S. Mahapatra, Prospects of zero Schottky barrier height in a graphene-inserted MoS2-metal interface, Journal of Applied Physics 119 (1) (2016) 014303. doi:10.1063/1.4938742.

[14] P.-C. Shen, C. Su, Y. Lin, A.-S. Chou, C.-C. Cheng, J.-H. e. a. Park, Ultralow contact resistance between semimetal and monolayer semiconductors, Nature 593 (7858) (2021) 211–217. doi:10.1038/s41586-021-03472-9.

[15] M. G. Pala, P. Giannozzi, D. Esseni, Unit cell restricted Bloch functions basis for first-principle transport models: Theory and application, Phys. Rev. B 102 (2020) 045410. doi:10.1103/PhysRevB.102.045410.

[16] P. Giannozzi, O. Andreussi, T. Brumme, O. Bunau, M. B. Nardelli, M. C. et al., Advanced capabilities for materials modelling with Quantum ESPRESSO, Journal of Physics: Condensed Matter 29 (46) (2017) 465901. doi:10.1088/1361-648x/aa8f79.

[17] P. Khakbaz, F. Driussi, P. Giannozzi, A. Gambi, D. Esseni, Simulation study of Fermi level depinning in metal-MoS_2 contacts, Solid-State Electronics 184 (2021) 108039. doi:https://doi.org/10.1016/j.sse.2021.108039.

[18] P. A. Khomyakov, G. Giovannetti, P. C. Rusu, G. Brocks, J. van den Brink, P. J. Kelly, First-principles study of the interaction and charge transfer between graphene and metals, Phys. Rev. B 79 (2009) 195425. doi:10.1103/PhysRevB.79.195425.

[19] E. N. Voloshina, A. Generalov, M. Weser, S. Böttcher, K. Horn, Y. S. Dedkov, Structural and electronic properties of the graphene/Al/Ni(111) intercalation system, New Journal of Physics 13 (11) (2011) 113028. doi:10.1088/1367-2630/13/11/113028.

[20] F. Driussi, P. Palestri, L. Selmi, Modeling, simulation and design of the vertical Graphene Base Transistor, Microelectronic Engineering 109 (2013) 338–341, insulating Films on Semiconductors 2013. doi:https://doi.org/10.1016/j.mee.2013.03.134.